Cohen, M.H.; Meier, D.L.; Arshakian, T.G.; Homan, D.C.; Hovatta, T.; Kovalev, Y.Y.; Lister, M.L.; Pushkarev, A.B.; Richards, J.L.; Savolainen, T.

Studies of the Jet in Bl Lacertae. I .Recollimation Shock and Moving Emission Features

Published in:
Astronomical Journal

DOI:
10.1088/0004-637X/787/2/151

Published: 01/01/2014

Document Version
Publisher's PDF, also known as Version of record

Please cite the original version:
Cohen, M. H., Meier, D. L., Arshakian, T. G., Homan, D. C., Hovatta, T., Kovalev, Y. Y., Lister, M. L., Pushkarev, A. B., Richards, J. L., & Savolainen, T. (2014). Studies of the Jet in Bl Lacertae. I .Recollimation Shock and Moving Emission Features. *Astronomical Journal*, (787), 10. https://doi.org/10.1088/0004-637X/787/2/151

The Astrophysical Journal, 787:151 (10pp), 2014 June 1 doi:10.1088/0004-637X/787/2/151

STUDIES OF THE JET IN BL LACERTAE. I. RECOLLIMATION SHOCK AND MOVING EMISSION FEATURES

M. H. Cohen[1], D. L. Meier[2], T. G. Arshakian[3,4], D. C. Homan[5], T. Hovatta[1,6], Y. Y. Kovalev[7,8], M. L. Lister[9], A. B. Pushkarev[8,10,11], J. L. Richards[9], and T. Savolainen[8]
[1] Department of Astronomy, California Institute of Technology, Pasadena, CA 91125, USA; mhc@astro.caltech.edu
[2] Jet Propulsion Laboratory, California Institute of Technology, Pasadena, CA 91109, USA
[3] I. Physikalisches Institut, Universität zu Köln, Zülpicher Strasse 77, D-50937 Köln, Germany
[4] Byurakan Astrophysical Observatory, Byurakan 378433, Armenia and Isaac Newton Institute of Chile, Armenian Branch, Chile
[5] Department of Physics, Denison University, Granville, OH 43023, USA
[6] Aalto University Metsähovi Radio Observatory, Metsähovintie 114, 02540 Kylmälä, Finland
[7] Astro Space Center of Lebedev Physical Institute, Profsoyuznaya 84/32, 117997 Moscow, Russia
[8] Max-Planck-Institut für Radioastronomie, Auf Dem Hügel 69, D-53121 Bonn, Germany
[9] Department of Physics and Astronomy, Purdue University, 525 Northwestern Avenue, West Lafayette, IN 47907, USA
[10] Pulkovo Observatory, Pulkovskoe Chausee 65/1, 196140 St. Petersburg, Russia
[11] Crimean Astrophysical Observatory, 98409 Nauchny, Crimea, Ukraine
Received 2013 December 19; accepted 2014 April 2; published 2014 May 14

ABSTRACT

Parsec-scale VLBA images of BL Lac at 15 GHz show that the jet contains a permanent quasi-stationary emission feature 0.26 mas (0.34 pc projected) from the core, along with numerous moving features. In projection, the tracks of the moving features cluster around an axis at a position angle of $-166.^{\circ}6$ that connects the core with the standing feature. The moving features appear to emanate from the standing feature in a manner strikingly similar to the results of numerical two-dimensional relativistic magneto-hydrodynamic (RMHD) simulations in which moving shocks are generated at a recollimation shock (RCS). Because of this, and the close analogy to the jet feature HST-1 in M87, we identify the standing feature in BL Lac as an RCS. We assume that the magnetic field dominates the dynamics in the jet, and that the field is predominantly toroidal. From this we suggest that the moving features are compressions established by slow and fast mode magneto-acoustic MHD waves. We illustrate the situation with a simple model in which the slowest moving feature is a slow-mode wave, and the fastest feature is a fast-mode wave. In the model, the beam has Lorentz factor $\Gamma_{\rm beam}^{\rm gal} \approx 3.5$ in the frame of the host galaxy and the fast mode wave has Lorentz factor $\Gamma_{\rm Fwave}^{\rm beam} \approx 1.6$ in the frame of the beam. This gives a maximum apparent speed for the moving features, $\beta_{\rm app} = {\rm v_{app}/c} = 10$. In this model the Lorentz factor of the pattern in the galaxy frame is approximately three times larger than that of the beam itself.

Key words: BL Lacertae objects: individual (BL Lacertae) – galaxies: active – galaxies: jets – magnetohydrodynamics (MHD) – waves

Online-only material: machine-readable table

1. INTRODUCTION

BL Lacertae objects are a class of active galactic nuclei (AGNs) that contain a relativistic narrow outflow (a jet) aimed close to the line of sight (LOS). This produces the characteristic features seen at radio wavelengths: high brightness temperature, rapid variability, and high polarization. Many of the BL Lacs are gamma-ray emitters. In high-resolution radio images, some show a sharply bent or kinked jet that changes on time scales as short as a year or less. In some cases bright features, or components, in the jet move downstream at nearly the speed of light c giving them a proper motion μ with an apparent speed $\beta_{\rm app} > 1$ (in units of c) in the coordinate frame of the galaxy. It is these rapid changes in the jet of the eponymous BL Lacertae itself that we investigate in this series of papers. In the current paper we consider the kinematics of the components, and we suggest that the quasi-stationary component is a recollimation shock (RCS), that the moving components emanate from the RCS, and that the moving components are magneto-acoustic waves. In the next paper (Paper II, in preparation) we show that the jet supports transverse waves as well, and suggest that they are Alfvén waves.

We need to distinguish between the pattern speed of a component and the speed of the beam itself (i.e., the bulk speed of the plasma). It is the latter that, through its Doppler factor, provides a relativistic boost to the flux density, and it is the former that gives the apparent motion. These speeds do not have to be the same, but it is often assumed that they are (e.g., Lister et al. 2009). In Section 4 we suggest that in BL Lac the moving components correspond to MHD waves traveling longitudinally in a helical magnetic field, and thus that the pattern and beam speeds are not the same.

We will need a value for θ, the angle between the jet axis and the LOS. To choose one we have investigated values based on statistics, and others based on observations of BL Lac as interpreted with synchrotron-emitting models of the core. The first statistical method is based on the maximum observed apparent speed, $\beta_{\rm app} = 10.0$ (Lister et al. 2013, hereafter L13), which gives an upper limit $\theta < 11.^{\circ}4$. However, a source selected on the basis of its beamed emission is highly unlikely to have θ near its extreme upper limit, because the flux density is strongly deboosted there. Roughly half of the sources in a beamed flux density-limited sample will have $\Gamma \sim \beta_{\rm app}$ and $\theta \sim 1/\Gamma$, while the most probable value of θ is $\sim 1/2\Gamma$ (Lister & Marscher 1997; Cohen et al. 2007). Also, Pushkarev et al. (2009, 2012) showed that the probability density function for θ for a subset of MOJAVE sources that were detected with the Fermi LAT has a peak near 2° and a median of 3°. BL Lac is in this group of

gamma-ray emitters. These studies suggest that θ is probably on the order of 3°.

On the other hand, Hovatta et al. (2009) have derived a value of $\theta = 7.^{\circ}3$ for BL Lac from the variability Doppler factor technique, and Jorstad et al. (2005, hereafter J05) have derived $\theta = 7.^{\circ}7 \pm 1.^{\circ}9$ using a light-travel time argument. These are remarkably close. Thus, measurements and synchrotron theory give $\theta \sim 7.^{\circ}5$, while probability arguments suggest $\theta \sim 3°$. Further observations that affect θ are of the position angle (P.A.) of the jet, which for BL Lac is variable and changes by up to 20° on timescales of five years (J05, L13). When this is deprojected it means that θ itself changes by a few degrees. Caproni et al. (2013) have studied these changes with a precession model, and find that θ changes by about 4° to 5°, apparently without crossing the LOS. In this paper, when necessary, we will assume $\theta \approx 6°$, and that the foreshortening is a factor of 10.

High-resolution observations at millimeter wavelengths show that, on a scale of 0.2 mas, the P.A. of the inner jet of BL Lac is variable (J05). These P.A. variations led to a suggestion by Stirling et al. (2003, hereafter S03) that the P.A. swings periodically, with a period of 2.3 ± 0.3 yr. This timescale was verified by Mutel & Denn (2005, hereafter MD05) who also said that the period was not unique, and that a period of 13.1 yr would fit as well. The Caproni et al. (2013) study yielded a precession period of 12.1 yr. In this paper we will show that on timescales of 1 to 12 yr the P.A. is variable but not periodic. The P.A. variations form an important part of our story, as they appear to be connected to the excitation of waves on the ridge line (Paper II).

Observational studies (Gabuzda et al. 2000; Lister & Homan 2005) have shown that the jets of BL Lac sources can be highly polarized, and that they have a bimodal distribution of electric vector position angle (EVPA) relative to the jet axis. In most cases the EVPA is longitudinal (i.e., roughly parallel to the axis), but in a small fraction of the cases it is transverse. Longitudinal EVPA is often interpreted as arising from an optically thin jet with a predominantly transverse magnetic field; although Lyutikov et al. (2005) have emphasized that this is not necessarily the case. For a relativistic beam, the ray path in the beam frame is perpendicular to the axis when $\theta = \theta_{\rm crit} \equiv \sin^{-1}(1/\Gamma)$ and in this case, when the field is helical with a high pitch angle and the jet is unresolved, the EVPA is longitudinal. However, the EVPA will vary as θ moves away from $\theta_{\rm crit}$. Transverse EVPA will be seen only for small θ (Lyutikov et al. 2005). If the jet is resolved, then for a helical field there should be a transverse gradient of rotation measure (RM; Blandford 1993). Gabuzda et al. (2004) tested this by measuring the RM in four BL Lacs, and they found indications of transverse gradients as expected for a helical magnetic field. However, this result is controversial as Taylor & Zavala (2010), using stricter criteria, did not detect a gradient of RM in four objects, including two of those studied by Gabuzda et al. (2004). This has been further studied by Hovatta et al. (2012) with extensive simulations of noise and other errors. They found a significant transverse gradient in four sources, of which two, 3C 273 (Asada et al. 2002; Zavala & Taylor 2005) and 3C 454.3 (Zamaninasab et al. 2013), have the signature expected for a helical field.

The evidence for a helical magnetic field in BL Lac comes from the high polarization and from the longitudinal EVPA. O'Sullivan & Gabuzda (2009a) have shown that its EVPA, corrected for rotation measure, remains longitudinal around a bend, and that at 7.9 GHz the polarization rises above 30%. Since the maximum polarization that can be attained by synchrotron radiation is 71% in a uniform magnetic field, in BL Lac the field must be well-ordered, at least in those parts of the jet where the polarization is high. From these studies, and because we can reasonably infer the existence of a helical field in both 3C 273 and 3C 454.3, we assume that in the jet frame of BL Lac the magnetic field basically has a helical shape, and that the pitch angle is not small.

The plan of this paper is as follows. In Section 2 we discuss the various bright features (components) in the jet (core, quasi-stationary, and moving) that are tracked by the MOJAVE program. In Section 3 we consider the quasi-stationary component near the core and why it is likely that it is an RCS. In Section 3.3 we extend this discussion to several other sources. In Section 4 we discuss the physical nature of the moving components in terms of fast and slow magneto-acoustic waves. Section 5 contains a discussion of our results, and conclusions are in Section 6.

BL Lac is nearby for a blazar ($z = 0.0686$) and our linear resolution is high (1 mas corresponds to 1.29 pc in the galaxy). This provides a great advantage to our study. Our second advantage is that BL Lac varies rapidly, and phenomena including P.A. variation and wave motion can be captured in a few years.

2. OBSERVATIONS

The MOJAVE program (Lister & Homan 2005, Monitoring of Jets in Active Galactic Nuclei with VLBA Experiments) is conducting regular observations of about 300 sources with the VLBA at 15 GHz (L13). The observing cadence varies from a few weeks for the most variable sources to about three years for slowly changing ones. BL Lac varies rapidly and we are currently observing it every one to two months. Here we present results from 55 epochs between 1996.2 and 2013.0. For this paper we have also added results from other programs whose results are in the VLBA archives, for a total of 110 epochs, all observed on the VLBA at a frequency near 15.3 GHz. See L13 for the most recent discussion of the MOJAVE program and its results, and for references.

We use multiple "snapshot" images from the VLBA in this paper. This involves observing BL Lac for a few minutes at each of a number of widely separated hour angles. The result has the full angular resolution of the VLBA, but there still may be gaps in the *uv*-plane coverage, due mainly to the wide separations of the fixed antennas. Figure 1 shows a 15 GHz image of BL Lac, made with the VLBA. It has a dynamic range of about 3000:1. The jet lies at a small angle θ to the LOS and the foreshortening is about a factor of 10. The jet is actually long and thin. At the epoch of Figure 1 it is reasonably straight, but at other epochs it is bent and sometimes kinked (L13).

We make a model of the source that consists of a set of Gaussian components (circular when possible) and have made tests of the modeling procedure by comparing results obtained by people working independently. In general, the stronger model components found with multiple snapshots are unique. Lister et al. (2013) showed that the accuracy of the locations of the centroids of the components, which is important for this paper, is about one-fifth the beamwidth, or about 0.1 mas EW by 0.2 mas NS, and for isolated bright components it is half that. We generally adopt ±0.1 mas as the accuracy.

The strong source at the north end of the jet is the core, and a prominent emission feature is seen at about 2 mas south of the core. This feature is a blend of two of the components in the

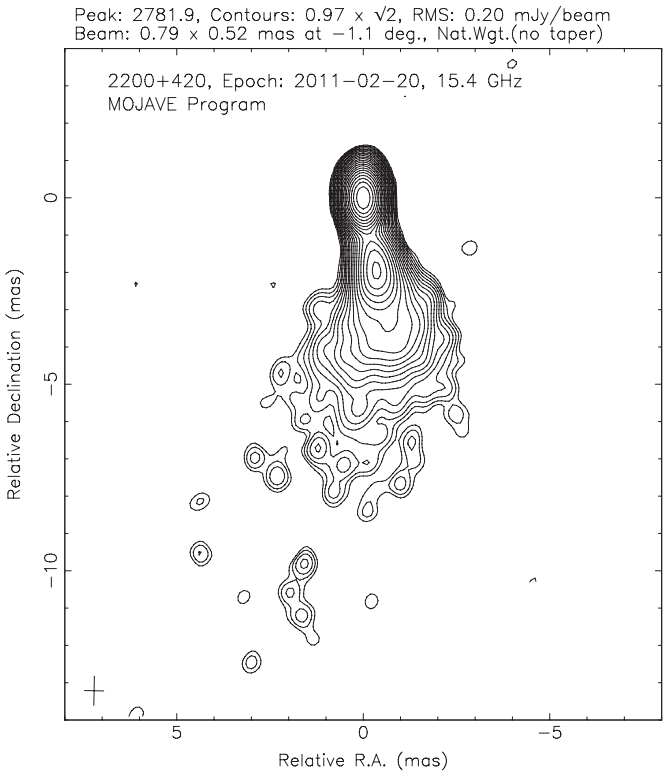

Figure 1. Image of BL Lac at 15.4 GHz, epoch 2011.14.

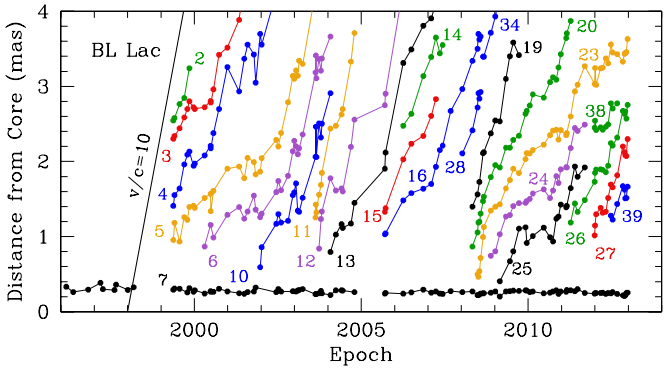

Figure 2. Separation of the components from the core. The straight black line has a slope corresponding to $\beta_{app} = 10$.

model for this epoch. In Figure 1 the jet widens near $r = 3$ mas and bends to the SE. This is seen in every 15 GHz image of BL Lac.

If the observational epochs are sufficiently close together the model components can be tracked without ambiguity, and they are generally seen to move downstream. We study each component and its motion carefully to decide if it is robust. This study includes an examination of the statistics of independent x and y fits of linear and acceleration terms to the motion. Further weight is given to the physical reality of a component when it has an identity that persists across a substantial frequency range. For example, in Section 2.3 we shall see that the 15–GHz component C2 has approximately the same location and motion as the 43 GHz component S10 (S03).

Table 1 gives the results of model-fitting Gaussian components to the (u, v) data. This table is similar to Table 4 in L13, with the data listed by component number, rather than by epoch. Most of the data here are the same as in L13, but because the database is continuously being augmented, revisions are introduced into some components. Thus the data here are not identical to the data in L13. Our final epoch for this paper is 2012 December 23. The temporal coverage prior to 1999 May is insufficient for robust cross-identification of jet features, so for those epochs in Table 1 we have listed only the data for the core and for component 7, which are valid.

Table 1
Fitted Jet Components

I.D.	Epoch	I (Jy)	r (mas)	P.A. (°)	Maj. (mas)	Ratio	Maj. P.A. (°)
(1)	(2)	(3)	(4)	(5)	(6)	(7)	(8)
0	1996-02-28	0.71	0.00	0.00	0.07	1.00	...
0	1996-05-16	1.69	0.00	0.00	0.00	1.00	...
0	1996-10-27	1.47	0.00	0.00	0.04	1.00	...
0	1997-03-10	1.09	0.00	0.00	0.00	1.00	...
0	1997-04-06	0.86	0.00	0.00	0.00	1.00	...
0	1997-08-10	1.25	0.00	0.00	0.06	1.00	...
0	1997-08-28	1.47	0.00	0.00	0.04	1.00	...
0	1998-01-03	1.27	0.00	0.00	0.03	1.00	...
0	1998-03-07	1.17	0.00	0.00	0.07	1.00	...
0	1999-01-02	1.20	0.00	0.00	0.06	1.00	...
0	1999-05-16	1.21	0.00	0.00	0.10	1.00	...
0	1999-05-29	1.17	0.00	0.00	0.09	1.00	...
0	1999-07-24	1.89	0.00	0.00	0.05	1.00	...
0	1999-09-12	1.93	0.00	0.00	0.23	1.00	...
0	1999-10-16	1.86	0.00	0.00	0.00	1.00	...
0	1999-11-06	2.06	0.00	0.00	0.00	1.00	...

Notes. Columns are as follows: (1) component identification number (zero indicates core component), (2) observation epoch, (3) flux density in Jy, (4) position offset from the core component in milliarcseconds, (5) position angle with respect to the core component in degrees, (6) FWHM major axis of fitted Gaussian in milliarcseconds, (7) axial ratio of fitted Gaussian, (8) major axis position angle of fitted Gaussian in degrees.
[a] Fewer than five epochs, or $r > 4$ mas.

(This table is available in its entirety in a machine-readable form in the online journal. A portion is shown here for guidance regarding its form and content.)

In this paper we restrict the discussion to physically plausible components by selecting only those that satisfy the following criteria: flux density $S_{15} > 20$ mJy and size (FWHM) < 2.0 mas, in addition to noise and reliability requirements. Furthermore, we flag and do not use components in Table 1 that are seen at fewer than four epochs, or have $r > 4$ mas. For 2005 July, the core was constrained to be circular to obtain a useful fit for Component 7. This means that the component positions in Table 1 for 2005 July may not be compatible with those for other epochs, particularly in solving for the kinematic properties as in Table 5 of L13.

Figure 2 shows the radial motion of 24 components of BL Lac. The straight line starting at (1998, 0) has a slope corresponding to $\beta_{app} = 10$, which is the value attained by component C1, although this is not seen in Figure 2 because it lies at $r > 4$ mas. The highest value seen in Figure 2 is $\beta_{app} = 9.2$, for component C11 (L13).

2.1. The Core

The core of a jetted radio source is generally defined as the compact flat-spectrum component seen at one end of the jet; it appears at nearly every epoch and is often assumed to be stationary on the sky. In Figure 1 the core is at the north end of the image and is the reference point for all other components. However, the absolute position of the core can depend on

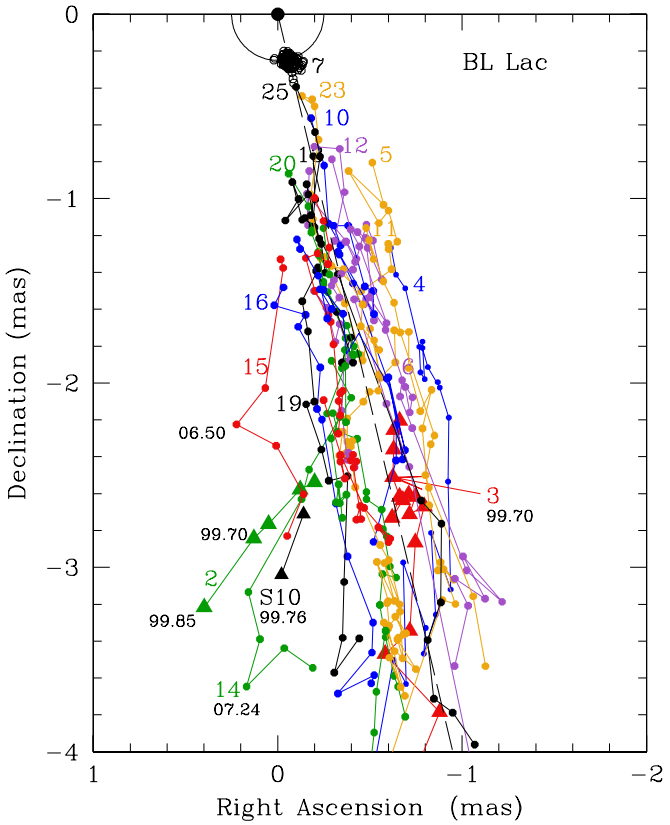

Figure 3. R.A.–Decl. tracks for the components, relative to the core at (0, 0). The circle at $r = 0.25$ mas is for convenience. The cluster of black points is component 7, which we identify as a recollimation shock. The E–W uncertainty is ±0.1 mas. The dashed line at P.A. $= -166.^{\circ}6$ is an axis that connects the core and the mean of component 7. The solid black triangles are for the 43 GHz component S10. See text.

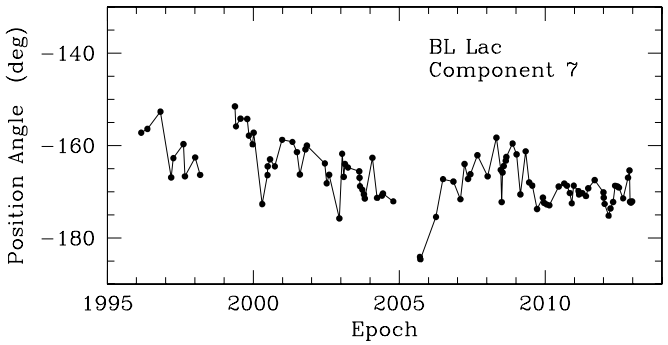

Figure 4. Position angle vs. epoch for component 7.

the observing frequency, since it is usually regarded as the photosphere (i.e., the $\tau \approx 1$ region in a smoothly varying jet; see e.g., Sokolovsky et al. 2011; O'Sullivan & Gabuzda 2009b, Kovalev et al. 2008). The measured core shift in BL Lac, between 8 and 15 GHz, is of order 50 μas (Pushkarev et al. 2012). Further, the core may prove to be a compound structure when viewed at a shorter wavelength, with more resolution and less opacity. This is the case for BL Lac, as we now show.

Independent 43 GHz VLBA observations of BL Lac were made by J05 and by MD05 over partly overlapping intervals between 1998 and 2003. Jorstad et al. (2005) show that BL Lac had three permanent components in the inner region: the 43 GHz core itself and two components to the south, labeled A1 and A2 (see J05, Figure 16). Mutel & Denn (2005) obtain a similar result; they see the same three components and call them C1, C2, and C3. S03 call the two northern components C1 and C2. To avoid confusion we will exclusively use the designations A0, A1, and A2 for the 43-GHz components, to refer to the core and the two components labeled A1 and A2 by J05. At 43 GHz A1 is substantially stronger than A0. We assume that A0 is the 43 GHz core of BL Lac, and A1 and A2 are stationary shocks in the jet. It is unlikely that A1 is the core and A0 is part of a counter-jet, because the Lorentz factor of the beam is of order 3 or more, and therefore there is an expected ratio of 10^3 or more between the flux densities of the jet and the counter-jet.

Jorstad et al. (2005) list the separations of A1 and A2 from A0 as 0.10 and 0.29 mas, respectively (J05, Table 5). S03 show that the P.A. from A0 to A1 is variable, between about -153° and -190°. It was this swing in P.A. that led them to suggest a periodicity. At 15 GHz, the angular resolution of the VLBA is insufficient to separate A0 and A1, and together they form the core at 15 GHz. The variable P.A. between A0 and A1, however, does mean that the 15 GHz core moves on the sky. The motion depends on the 15 GHz flux density ratio between A0 and A1; this is unknown, but at 43 GHz A1 is substantially stronger than A0 (J05, MD05). In any event, the position shift will mainly be in the R.A. direction and the sky motion will be $\leqslant 60\,\mu$as y^{-1}. This is consistent with the proper motion measured at 8 GHz from 1994 to 1998: $20.4 \pm 6.6\,\mu$as yr^{-1}, at P.A. $= -16 \pm 16^{\circ}$ (Moór et al. 2011). The accuracy of our position measurements is estimated to be ±0.1 mas, so we ignore the possible shifts in the apparent core position.

2.2. The Quasi-Stationary Component

At 15 GHz BL Lac contains a quasi-stationary component, C7, seen in Figure 2 at about 0.26 mas from the core. In Figure 3, an R.A.–Decl. plot, C7 is seen as the tight cluster of points with a centroid at $r = 0.26$ mas and a position angle P.A. $= -166.^{\circ}6$. This is close to the location of the 43 GHz component A2 from its core, $r = 0.29$ mas, P.A. $\approx -166^{\circ}$. We therefore identify C7 with the 43 GHz component A2. The small difference in radius at the two frequencies can be attributed to the compound nature of the core as described above.

The 15 GHz restoring beam of the VLBA for BL Lac, calculated with naturally weighted data, is roughly 0.9×0.6 mas (FWHM) at P.A. $= -9^{\circ}$, so that the separation between the core and C7 is less than the beam size. Such super-resolution generally leads to a non-unique model, whose utility depends on the SNR and on the true level of complication in the field. In our case the SNR is high, and from the 43-GHz observations we know that there is only a small number of compact components in the field. Hence we have an apriori case that superresolution is reasonable. We also justify our superresolution by the good agreement for the positions of components C7 and A2 at 15 and 43 GHz.

In Figure 4 we show the P.A. of C7 relative to the core as a function of time. The P.A. is stable after about 2009.5, and the scatter there is an indication of the noise in the measurements, which appears to be about $\pm 3^{\circ}$. There is no periodicity that is apparent on scales from 1 to 12 yr, but longer periods are not excluded. MD05 (their Figure 3) show the combined S03 and MD05 data at 43 GHz for the P.A. close to the core. Their data closely match ours for the overlap period, 1999.0–2002.0, with a lag of a few months for the 15 GHz data. This good agreement is further justification for superresolution, and for using ±0.1 mas as a conservative estimate of the error in the positions of the components.

It is not unusual to see a quasi-stationary component in a jetted source, but the tightness of the cluster of points for C7 is remarkable. In Figure 4 the RMS scatter in the R.A. and Decl. positions, relative to the mean, is 30 μas and 28 μas, respectively. The net vector proper motion is 3.8 ± 0.6 μas y^{-1} at P.A. $= 82^\circ \pm 10^\circ$ (L13).

2.3. The Moving Components

The slope μ for a component in Figure 2 gives its apparent radial speed, calculated as $\beta_{\rm app} = \mu RD(1+z)$ where $\beta_{\rm app}$ is relative to c the speed of light, μ is in mas y^{-1}, D is the angular diameter distance in light-years, and R converts mas to radians. See Homan et al. (2009), who discuss the definition of speed and acceleration. It is clear that in BL Lac there is a wide distribution of speeds, but it is the fastest one that is usually quoted. This honor goes to component C1, which has the value $\beta_{\rm app} = 10.0$ (L13), although this component has $r > 4$ mas and is outside the purview of this paper.

Nineteen of the moving 15 GHz components are shown in Figure 3. Five of the components in Figure 2 are not shown because they have only four or five epochs each and merely add to the general group of unmarked sources near the axis. The dashed line at P.A. $= -166.^\circ6$ runs from the core through the mean of C7. This axis is roughly parallel to the tracks of the moving components, which surround it in a somewhat symmetrical fashion, except for components C2, C14, and C15. The moving components all appear to start downstream of C7. There is no indication that there are moving components upstream from C7, although we have little angular resolution there. This bears a close resemblance to the moving shocks generated by the stationary RCS in the numerical simulations by Lind et al. (1989), which we discuss in Section 3.1. At 43 GHz the situation is similar, except for one episode in 2005 when a moving component was seen traveling superluminally from the core to C7 (Marscher et al. 2008). This suggests that the 43 GHz core itself may possibly be an RCS, and that higher frequency studies may be needed to sort out this situation.

Most of the moving components start near $r = 0.8$ mas, with only three, C10, C23, and C25, clearly appearing before $r = 0.6$ mas. This may be due to sensitivity, with most components being born weak and only rising to a measureable flux level after traveling several parsecs. Or, it might represent a jet phenomenon. This shortage of flux close to component 7 has been discussed by Bach et al. (2006). Note also that components C10, C23, and C25, which are close to the core, start close to the axis at P.A. $= -166.^\circ6$, whereas those that start farther downstream are spread across 0.5 mas surrounding the axis.

Tateyama (2009), using VLBA archival data at 8 and 15 GHz, described the motions in BL Lac as a succession of ballistic components traveling through a narrow stationary window to the south, running from about 1 to 2 mas. That description is generally consistent with our Figure 3. Caproni et al. (2013) have published a study of BL Lac that includes an R.A.–Decl. plot like that in Figure 3, but for 311 points at six frequencies from 5 to 43 GHz, all taken from the literature, and all obtained with VLBI between 1979 and 2008. Their Figure 1 is similar to our Figure 3, but their individual components are not followed in time.

On the west side of the tracks in Figure 3, components C4 and C5 form an envelope that is roughly parallel to the axis. On the east side, however, there are several components, C2, C14 and C15, with large transverse excursions. The 43-GHz component S10 similarly has a large eastern excursion, and two points from the data listed by S03 are included in Figure 3, as the solid black triangles. The final points for C2 and S10 are labeled with their epochs. They are close enough together in both space and time that we identify them as the same component, with the spatial difference probably due to a spectral gradient. The independent 15 and 43 GHz observations show that C2 and S10 are real, and not artifacts of the observations or reductions. Component 14 occupies the SE region taken by C2, but seven years later.

Component C2 is contemporaneous with the early part of component C3, which is labeled with the arrow in Figure 3, and shown as the large red triangles. C3 stays close to the axis, while C2 moves to the SE. Unfortunately, we only have limited 15 GHz observations immediately prior to 1999, so we cannot see if C3, moving radially, spawned C2, which moved with a large transverse component.

These excursions of the moving components away from the axis are all on the east side, which is in the direction of the general bend in the source seen at $r > 3$ mas in Figure 1. The character of the source changes near 3 mas: the narrow jet becomes a broad low-surface brightness extended region without a sharp ridge. The components there may not be on a pressure maximum and may have a different character from the ones on the narrow ridge closer to the core.

3. THE QUASI-STATIONARY COMPONENT AS A RECOLLIMATION SHOCK

A "master" recollimation, or reconfinement, shock (RCS) is a natural, quasi-stationary feature of an MHD wind/jet that is expected to form beyond the "final critical point"—the place where the accelerating and collimating flow becomes causally disconnected from the central engine. Sometimes called the modified fast point (MFP), the final critical point was ignored in early studies of jet acceleration (Blandford & Payne 1982; Li et al. 1992); and even the more recent Vlahakis & Königl (2003), who assumed that the MFP lay infinitely far from the central black hole. However, the MFP has been studied extensively by Vlahakis et al. (2000) and Polko et al. (2010, 2013a, Polko et al. 2014) who showed that it can lie at a finite distance within a galactic nucleus (e.g., $\lesssim 10^6\, r_g$ or parsec scale, where $r_g = {\rm GM_{BH}/c^2}$ is the black hole gravitational radius). At the MFP the jet has a strong, toroidally dominated magnetic field, the forward flow is highly *super-magnetosonic* and converging, and even that flow *toward* the central jet axis exceeds the magnetosound speed. Within less than a magnetosound crossing time, the flow will converge beyond the final critical point into a strong compressive recollimation wave or shock.

3.1. Theoretical MHD Simulations of the RCS

Helical field dominated, super-magnetosonic flow like that expected beyond the MFP has been studied extensively, with both nonrelativistic and relativistic, two-dimensional MHD simulations (Clarke et al. 1986; Lind et al. 1989; Komissarov 1999; Krause & Camenzind 2001). A strong MHD pinch shock indeed forms quickly, and just beyond it a magnetic chamber that alternately opens and closes, ejecting new jet components forward at trans- (not super-) magnetosonic speeds. Since, to our knowledge, super-magnetosonic, helically dominated MHD jets have not yet been studied in three-dimensional simulations, the details of these results must be considered tentative only. However, it is clear from all the simulations that the RCS dramatically changes the character of the flow, giving birth to a new and more stable *trans*-magnetosonic jet

Table 2
Distance to Recollimation Shock

Name	z	Class	pc/mas	theta	Dist to Shock	log M_{BH}	log R	Ref.
BL Lac	0.0686	BLL	1.29	6	0.26	8.2	5.6	1, 2
M87	0.00436	FR I	0.08	13	860	9.5	6.0	1, 3, 4
3C 120 S1	0.033	FR I	0.65	16	0.7	7.8	5.7	5, 6
3C 120 C80	...	...	...	...	80	...	7.8	6, 7
3C 273	0.158	FSRQ	2.70	6	0.15	9.8	4.1	8, 9
3C 390.3 S1	0.0561	FR II	1.09	50	0.28	8.6	4.3	10, 11

Notes. Columns are as follows: (1) common name, (2) redshift, (3) BLL = BL Lacertae object, FR I = Fanaroff–Riley type I, FSRQ = flat-spectrum radio quasar, and FR II = Fanaroff–Riley type II, (4) linear scale, (5) angle of inclination of jet to the LOS, (6) projected distance to shock in mas, (7) log mass of the black hole, (8) log deprojected distance to shock in gravitational radii, (9) references.
References. (1) This paper, (2) Woo & Urry 2002; (3) Cheung et al. 2007; (4) Gebhardt et al. 2011; (5) León-Tavares et al. 2010; (6) Grier et al. 2012; (7) Agudo et al. 2012; (8) Jorstad et al. 2005; (9) Paltani & Türler 2005; (10) Wandel et al. 1999; (11) Arshakian et al. 2010.

from the previously unstable super-magnetosonic pre-shock jet. See Meier (2012, Section 15.2.2.2) and Meier (2013) for a more detailed discussion.

3.2. Comparison with M87

The jet of M87 contains a quasi-stationary emission region called HST-1, $\geqslant$120 pc from the BH, and several superluminal components ($\beta_{\rm app,max} = 4.3$) downstream from HST-1 (Cheung et al. 2007; Chang et al. 2010). Cheung et al., also Stawarz et al. (2006) and Bromberg & Levinson (2009) discuss HST-1 as a reconfinement or recollimation shock generated by a change in the gradient of the external pressure, and they suggest that the superluminal components are generated in the HST-1 shock.

Component 7 of BL Lac is analogous to HST-1 in M87. It is quasi-stationary, and, as shown in Figure 3, the superluminal components appear to emanate from it, although there is not enough angular resolution to state definitively that none of the moving components start upstream of C7. At 43 GHz there is more angular resolution. J05 (their Figure 16) show three superluminal components that all start near component A2 (same as the 15 GHz component C7). Additionally, Marscher et al. (2008) report an exceptional event in 2005, in which a 43 GHz component appeared to start slightly upstream of the core, and was tracked, moving superluminally, to component A2.

Table 2 summarizes the details of the shocks in these sources, and the others in Section 3.3. The objective of the Table is to compare the distances (in gravitational radii) of the putative RCS from the SMBH, in column 8. These values have a large uncertainty, perhaps 0.6 dex.

To calculate the distance we must assume values for the inclination angle θ and for $M_{\rm BH}$. For BL Lac, we assume $\theta \approx 6^\circ$ as described above, and we take $\log M_{\rm BH}/M_\odot = 8.2$ from Woo & Urry (2002). This is lower than the typical values of $M_{\rm BH}/M_\odot$ for BL Lacs reported by Falomo et al. (2002), $\log M_{\rm BH}/M_\odot \sim 8.6$, but their sample was small and had a large variance, and did not include BL Lac. Using $\log M_{\rm BH}/M_\odot = 8.2$ gives $R \sim 4 \times 10^5\, r_g$. This value is uncertain enough that there is no need to consider adding the distance of the core from the BH itself.

For M87 Cheung et al. (2007) derive a limit to the deprojected distance of HST-1 by using the maximum observed superluminal speed and the corresponding maximum angle to the LOS, 26°. In our opinion the maximum angle is unrealistic, and it is preferable to estimate the distance by using the angle that minimizes the Lorentz factor, $\theta = 13^\circ$. M87 is not selected on the basis of its beamed flux density as is BL Lac, and it would be inappropriate to use a further reduction in the angle. Thus we adopt R = 300 pc as the de-projected distance from the BH to HST-1. The mass of the BH in M87 is estimated as $6.6 \times 10^9\, M_\odot$ (Gebhardt et al. 2011), giving a distance to HST-1 of about $10^6\, r_g$. Component 7 in BL Lac and HST-1 in M87 are both quasi-stationary, and are at similar gravitational distances from their black holes. In both objects, the major superluminal motions are seen downstream of the stationary component. HST-1 is presumed to be an RCS and we suggest that component 7 is one, also.

In the Lind et al. (1989) strong-field, super-magnetosonic simulations, successive pairs of shocks appear downstream of the RCS. They move in a narrow "nose cone" (a post-RCS, trans-magnetosonic flow) where the pressure is much higher than it is in the surrounding cocoon, due to plasma confinement by a toroidal magnetic field. We have suggested that C7 in BL Lac is an RCS, and we now suggest that the fast components downstream of C7 are *moving* shocks in this post-RCS flow.

The comparison of the BL Lac observations with the Lind et al. (1989) simulations is striking and lends credence to the idea that C7, like HST-1 in M87, is indeed an RCS. However, some details, including the transverse excursions seen in Figure 3, have no analog in the axisymmetric simulations.

3.3. Quasi-Stationary Components in Other AGN

Many AGN show quasi-stationary components in parsec-scale images (see e.g., J05, Figure 16 and L13, Figure 3). In this section we briefly discuss such components in two radio galaxies, 3C 120 and 3C 390.3, and one quasar, 3C 273. Their details are in Table 2. 3C 120, like M87, is an FR I radio galaxy and these objects, according to standard unification theory, are the parent population of the BL Lacs. MOJAVE images at 15 GHz show that 3C 120 has a quasi-stationary component, called S1 by León-Tavares et al. (2010), 0.7 mas from the core. Taking $\theta \approx 16^\circ$ (Agudo et al. 2012) and $M_{\rm BH} \approx 6.7 \times 10^7\, M_\odot$ (Grier et al. 2012) gives $R \approx 5 \times 10^5\, r_g$.

In 3C 120 numerous radio components seen at 15 GHz appear to start at or near S1 and move superluminally downstream (León-Tavares et al. 2010). At 43 GHz, however, (Gómez et al. 2001; Jorstad et al. 2005) it is seen that several components start close to the core and pass through S1. This difference may be due to the differing angular resolutions, but may also be due to the spectra of the components, which may be strongly inverted when the components first come out of the core. In addition, 3C 120 had five or six optical flares that were closely correlated in time to the back-extrapolated passage of the 15 GHz superluminal components through the component S1 (León-Tavares et al. 2010). The flares were not well-correlated with the times when

the back-extrapolated superluminal components were at the core. During the appropriate time period there were seven radio components, so it appears that the correspondence between the optical flares and the times when the superluminal radio components were at S1 is good. León-Tavares et al. discuss the statistics of this association.

Table 2 shows that S1 in 3C 120 is at a distance from the BH that is comparable to those of HST-1 for M87 and C7 for BL Lac; superluminal components from the nearby core move through it, and it appears to have a connection with optical flare events. We agree with León-Tavares et al. (2010) that S1 is probably an RCS.

3C 120 also has a quasi-stationary component 80 mas from the core, and Agudo et al. (2012) suggest that it is an RCS. However, this component is 1–2 orders of magnitude farther from the BH than are the other RCS in Table 2, and furthermore the main superluminal components in 3C 120 lie far *upstream* from C80. We therefore suggest that component C80 in 3C 120 is of a different character from HST-1 in M87, C7 in BL Lac, and S1 in 3C 120.

3C 273 is a flat-spectrum radio quasar that has a quasi-stationary component in its jet at 0.15 mas from the core, seen in VLBA images at 43 GHz (Jorstad et al. 2005; Savolainen et al. 2006). Estimates of θ in the literature range from 3.°3 (Hovatta et al. 2009) to 10°(Savolainen et al. 2006); for this paper we will use $\theta \approx 6^\circ$ (J05). Using $M_{\rm BH} \approx 6.6 \times 10^9\, M_\odot$ (Paltani & Türler 2005) gives $R \approx 1.2 \times 10^4\, r_g$. This value for R/r_g is about two orders of magnitude smaller than the values for BL Lac, M87, and 3C 120. The low distance estimate does not preclude its being an RCS, but it may be of a different character from those discussed above. Another difference is that, like many radio loud quasars, 3C 273 has a predominantly transverse EVPA in the jet, whereas the BL Lac objects have a predominantly longitudinal EVPA.

3C 390.3 is an FR II radio galaxy with a jet that has $\Gamma \sim 2$ and $\theta \sim 50^\circ$ (Arshakian et al. 2010). Arshakian et al. (2010) combined their 15 GHz VLBA observations with observations made by the MOJAVE group, for a total of 21 epochs from 1994 to 2008. They identified a quasi-stationary component (S1) 0.28 mas from the core. Taking $M_{\rm BH} \sim 4 \times 10^8\, M_\odot$ (Wandel et al. 1999) gives $R/r_g \sim 2 \times 10^4$. This value is comparable to the value for 3C 273 and smaller than the others. Again, this difference does not disqualify S1 from being an RCS, but it may have a different character from those in M87, BL Lac, and 3C 120.

In 3C 390.3 numerous 15 GHz components appear to arise within a few tenths of a parsec of S1 and move downstream with $\beta_{\rm app} \sim 1$. During 1994 to 2008, 3C 390.3 had eight optical or UV flares, and their peaks occurred close to the times when the back-extrapolated moving components were at the location of S1 (Arshakian et al. 2010). The flares were not well-correlated with the times when the back-extrapolated moving components were at the core. This behavior is like that in 3C 120. The flares appear to be connected with the passage of the superluminal components through S1.

4. THE MOVING COMPONENTS AS PROPAGATING MAGNETO-ACOUSTIC MHD WAVES OR SHOCKS

In Section 1 we briefly reviewed the subject of polarization in BL Lacs to justify our assumption that the magnetic field in the jet is in the form of a helix with a high pitch angle. We also assume that the magnetic pressure is stronger than the plasma fluid pressure. This allows us to invoke MHD to explain the observed phenomena. The conditions in the post-shock jet in the MHD RCS simulations discussed in Section 3.1 are surprisingly similar to the actual state of the BL Lac jet downstream from Component 7. In the simulations, the RCS is essentially non-dissipative, the new trans-magnetosonic jet still has a strong magnetic field (strong in the sense that the field contributes significantly to the jet dynamics), and the field retains its helical configuration. Furthermore, such a jet should display both kinds of classical magneto-acoustic waves (and shocks)—the MHD slow and fast modes—particularly along the jet axis. These waves are disturbances in the longitudinal direction, or *P* (pressure) waves. In this section we discuss slow and fast magneto-acoustic waves that, we suggest, form the moving components in the jet.

4.1. Slow MHD Waves and Shocks in the BL Lac Jet

Classical slow MHD waves are the lower branch of the magneto-acoustic modes. They compress only the jet plasma and not the magnetic field, and they propagate with a phase speed of only

$$V_S = \pm \left\{ \frac{1}{2} \left[c_{ms}^2 - \left(c_{ms}^4 - 4\, c_s^2\, V_A^2\, \cos^2\, \chi \right)^{1/2} \right] \right\}^{1/2} \qquad (1)$$

where χ is the angle between the wave propagation and magnetic field directions, $V_A \equiv B/(4\pi\rho)^{1/2}$ is the scalar Alfvén speed, $c_s \equiv (\gamma p/\rho)^{1/2}$ is the plasma sound speed, $c_{ms} \equiv (V_A^2 + c_s^2)^{1/2}$ is the magnetosound speed, and B, p, ρ, and γ are the magnetic field strength, plasma pressure, mass density, and adiabatic index, respectively. Note: for the sake of straightforward discussion, we give here, and in Equation (2) below, the nonrelativistic versions of the slow and fast wave expressions. The full relativistic versions (again in the fluid frame) are given in the Appendix and are used in our actual computations.

Note that the propagation speed of the slow wave depends on whether the magnetic forces internally dominate the plasma or vice versa and on the angle χ of propagation of the wave to the magnetic field. In our magnetic model for BL Lac ($V_A^2 \gg c_s^2$) the (nonrelativistic) slow wave speed is given by $V_S \approx (c_s V_A/c_{ms}) \cos\chi \sim c_s \cos\chi$. So, the slow wave is a simple sound wave ($V_S = c_s$) *along* the magnetic field, but it propagates more slowly when it is skew to the field and has $V_S = 0$ normal to it. Slow MHD shocks can also occur, propagating at speeds faster than V_S.

Slow MHD waves propagating along the axis of the BL Lac jet through the helical magnetic field will have a very slow speed in the frame of the jet for two reasons. First, the wave will be traveling skew to the helical field, so its speed will be even less than the sound speed (because $\cos\chi$ could be much less than unity); and, second, if the field dominates, the sound speed could be quite low, so that $V_S < c_s \ll V_A$. Since slow MHD waves/shocks still compress the plasma (but not the field), they should produce a visible enhancement in the local synchrotron emission in the jet. However, that emission could be almost stationary with respect to the moving jet and mainly reflect the speed of the jet plasma beam when measured by the observer. Waves of this type would conform to the idea that the moving components travel with the beam, and that the Lorentz factor of the beam can be found from the speed of the components. This use of the slow magneto-acoustic mode could provide a justification for saying that the pattern speed equals the beam speed, in the proper circumstances.

4.2. Fast MHD Waves and Shocks in the BL Lac Jet

The upper branch of the magneto-acoustic modes, the fast MHD wave, compresses not only the plasma but also the magnetic field itself. Its propagation phase speed is given by the *positive* root of the dispersion relation,

$$V_F = \pm \left\{ \frac{1}{2} \left[c_{ms}^2 + \left(c_{ms}^4 - 4\, c_s^2\, V_A^2\, \cos^2\, \chi \right)^{1/2} \right] \right\}^{1/2} \quad (2)$$

When the magnetic field dominates and the Alfvén speed exceeds c_s, the speed of this wave is a very fast $V_F = V_A$ along the magnetic field, and normal to the field an even faster $V_F = c_{ms}$.

In contrast to the slow mode, fast MHD waves have no problem propagating along the jet axis at high speeds. In fact, if the helical field is in a fairly tight coil, $\cos^2 \chi$ will be small, and the fast wave speed will approach the full magnetosound speed. Furthermore, fast MHD shocks with $V_{\rm shock} > V_F$ are quite possible, most probably occurring when a new, strong blast of plasma attempts to propagate up the magnetic coil.

Fast MHD waves, therefore, are likely to be responsible for the fastest moving components in BL Lac. In addition, because of their ability to compress the fairly strong magnetic field, they fit well into the model for synchrotron emission that has been applied to BL Lac by Hughes et al. (1989). The only difference is that the initial field here is in an ordered helix, not in a tangled configuration.

4.3. A Simple MHD Model for the Moving Components

The considerable variation in the speeds of the components in Figure 2 is commonly seen in superluminal sources (L13), and the reasons usually given for this are that the components are due to shocks of different strength, that θ is variable, or that there are sub-beams of varying speed and direction. Here we suggest a slightly different model in which the speed of the waves or shocks that form the components may vary, largely because they are of two different wave or shock types (slow and fast magneto-acoustic waves), in addition to there being different speeds within the two classes. The detailed distribution of speeds is presumed to be set by variability at the RCS. Also, we assume that the speed of the beam and the viewing angle θ are fixed, the latter at 6°.

The model has two steps: (1) assume that the slowest speed in Figure 2 results from a slow mode wave of negligible speed in the jet frame and, from this, calculate the beam speed; (2) assume that the fastest speed in Figure 2 results from a fast mode wave traveling on the beam that, in turn, has the speed found in (1). This gives the speed of the fastest fast wave.

The model has three important speeds: $\beta_{\rm beam}^{\rm gal}$, the speed of the beam in the galaxy frame, and the speed of the wave in the beam and galaxy frames, $\beta_{\rm wave}^{\rm beam}$ and $\beta_{\rm wave}^{\rm gal}$. These are related by the relativistic velocity addition formula

$$\beta_{\rm wave}^{\rm gal} = \frac{\beta_{\rm wave}^{\rm beam} + \beta_{\rm beam}^{\rm gal}}{1 + \beta_{\rm wave}^{\rm beam} \beta_{\rm beam}^{\rm gal}} \quad (3)$$

In addition, $\beta_{\rm wave}^{\rm gal}$ is related to the observed $\beta_{\rm app}$ by the formula

$$\beta_{\rm app} = \frac{\beta_{\rm wave}^{\rm gal} \sin\theta}{1 - \beta_{\rm wave}^{\rm gal} \cos\theta} \quad (4)$$

and each speed has a corresponding Lorentz factor $\Gamma = (1 - \beta^2)^{-1/2}$.

Now assume that the slowest speed in Figure 2 represents the apparent speed of the slowest slow wave on the beam. From Figure 2 we choose the propagation of C5 from about 1999 to 2001 to represent the speed of the jet plus the slowest slow wave, or $\beta_{\rm app,Swave}^{\rm gal} = 2.1$. From Equation (4) with $\theta = 6°$, $\beta_{\rm Swave}^{\rm gal} = 0.958$ and $\Gamma_{\rm Swave}^{\rm gal} = 3.5$. We now assume the limiting case in which the slow wave speed (Equation (1)) is small in the frame of the beam, or $\beta_{\rm Swave}^{\rm beam} \sim 0$. This gives us the beam speed itself, $\beta_{\rm beam}^{\rm gal} \approx 0.958$ or $\Gamma_{\rm beam}^{\rm gal} \approx 3.5$. In this model, the slowest observed component indicates the actual speed of the beam.

The magnetosound speed in the jet can then be found by assuming that the fastest observed component speed is due to the fastest fast magneto-acoustic wave, or $\beta_{\rm app,Fwave}^{\rm gal} = 10$. Then, from Equation (4), $\beta_{\rm Fwave}^{\rm gal} = 0.995$ and $\Gamma_{\rm Fwave}^{\rm gal} = 10.1$. Inverting Equation (3) and taking $\beta_{\rm beam}^{\rm gal} \approx 0.958$ gives $\beta_{\rm Fwave}^{\rm beam} \approx 0.793$ and $\Gamma_{\rm Fwave}^{\rm beam} \approx 1.6$.

In this model the beam is relativistic, $\Gamma_{\rm beam}^{\rm gal} \approx 3.5$, the fast MHD wave is mildly relativistic in the beam frame, $\Gamma_{\rm Fwave}^{\rm beam} \approx 1.6$, and the slow MHD wave has negligible speed relative to the plasma. However, while this model assumes that in the jet the internal magnetic forces dominate the plasma forces ($V_A > c_s$), there is no information about the configuration or orientation of the magnetic field relative to the jet flow. This can be determined from the propagation of Alfvén waves, but such waves are not considered in this paper. They will, however, be presented in Paper II.

The beam itself has $\Gamma_{\rm beam}^{\rm gal} \approx 3.5$, a value lower than has been found in some other studies (e.g., Caproni et al. (2013) who find $\Gamma_{\rm beam}^{\rm gal} \approx 5.4$). However, our value is adequate to suppress the flux density from the counter jet (see Figure 1). For $\Gamma_{\rm beam}^{\rm gal} \approx 3.5$ and $\theta = 6°$ the Doppler factor $\delta \approx 6$, and the jet to counter-jet flux-density ratio is of order $\delta^{4-2\alpha} \sim 10^4$, taking the spectral index of the jet as $\alpha = -0.55$ (Hovatta et al. 2014).

Note that relativistic velocity addition is highly nonlinear. For the fast wave, $\Gamma_{\rm Fwave}^{\rm beam} \approx 1.6$ and $\Gamma_{\rm beam}^{\rm gal} \approx 3.5$; the combination gives $\Gamma_{\rm Fwave}^{\rm gal} \approx 10$. Here is a case where the Lorentz factor for the pattern is three times that for the beam. This is a general result and does not depend on the strength of the magnetic field in the jet model. For example, models for blazars with weak, tangled fields that are compressed by propagating shocks can also have moderate beam Lorentz factors with mildly relativistic shocks in the jet frame, and yet produce very fast, highly relativistic component speeds in the observer's frame.

5. DISCUSSION

The results presented in this paper may have rather wide application because there are theoretical reasons for believing that all extragalactic jets may have strong magnetic fields (relative to the kinetic pressure) and an RCS (Meier 2013). The objects in Table 1 are close to the Earth so the linear resolution on them is good, and yet the RCS in BL Lac is at the limit of angular resolution at 15 GHz. Thus higher frequencies or space VLBI will be necessary to study many more AGN, and to look for evidence of an RCS. The characteristics to look for in nearby objects are a stationary and bright feature (the candidate RCS) $\lesssim 10^6\, r_g$ from the core, a transverse magnetic field in that

feature, and superluminal components that appear to emanate from the RCS.

We included the class of each of the five objects in Table 2 in Column 3. Standard arguments (e.g., Chiaberge et al. 2000) based on orientation unify BL Lacs with FR I objects, and flat-spectrum radio quasars (FSRQ) with FR II objects. Thus, we consider BL Lac, M87 and 3C 120 as one group, and 3C 273 and 3C 390.3 as another. Column 8 of Table 2 shows that the RCS in the FSRQ/FR II group is one to two orders of magnitude closer to the BH than those in the BL Lac/FR I group (component C80 in 3C 120 is excluded from this comparison; see Section 3.3). Although the statistics of this comparison are weak, the result is interesting and suggests that the inner jets in the two groups of sources may differ in some way. In addition, these groups are not magnetically homogeneous. BL Lac has longitudinal EVPA but 3C 120 has transverse EVPA; Gómez et al. (2008) suggest that this is caused by a helical magnetic field of low pitch angle. M87 is unpolarized near the core at 15 GHz (Zavala & Taylor 2002). At HST-1 (the RCS) the RM-corrected EVPA is longitudinal, but it is transverse between the knots. 3C 273 displays a transverse gradient in its RM (Zavala & Taylor 2005; Asada et al. 2008; Hovatta et al. 2012) that suggests it has a helical magnetic field whose pitch angle is not small. Although the conventional picture says that this should result in a longitudinal EVPA, in fact the EVPA is predominantly transverse in 3C 273. For 3C 390.3 any polarized flux is undetectable (i.e., weak Taylor et al. 2001), as it is in most radio galaxies (Lister & Homan 2005).

In making the model we used in Section 4.3 we assumed that the speed of the beam is constant. This is unlikely to be true, but it is convenient and provides a way to estimate the speeds of the beam and the fast-mode wave. We can set a lower limit for the beam speed as follows. BL Lac is strongly one-sided and the jet-to-counterjet flux–density ratio is of order 10^3 or more. The appropriate limit, assuming BL Lac has symmetric opposite beams, is $\delta^{4-2\alpha} > 1000$ where δ is the Doppler factor and $\alpha = -0.55$, and so $\delta > 3.9$ and $\Gamma_{\rm beam} > 2$. If we use the value $\theta = 6^\circ$ then there is an upper limit, found by noting that the MHD waves propagate downstream on the beam, increasing the net speed seen by the observer. The fastest observed speed is $\beta_{\rm app} = 10$, and with $\theta = 6^\circ$ this gives $\Gamma_{\rm beam} < 10$. If we relax the condition $\theta = 6^\circ$, then there is no upper limit within this geometric framework.

The observed pattern is faster than the beam, for a component generated by a fast-mode MHD wave. For the particular model we have used, the fastest observed superluminal component has $\Gamma^{\rm gal}_{\rm Fwave} \approx 10$, and $\Gamma^{\rm gal}_{\rm beam} \approx 3.5$. The pattern is approximately three times faster than the beam. This result has consequences for unification theory, if it is confirmed. The standard picture says that BL Lacs and FR I galaxies form one class, with BL Lacs seen end-on and FR I's seen closer to the equatorial plane. Analyses based on this idea have difficulties, however, in that some properties, including luminosity ratios and superluminal motion, overpredict the amount of radio flux that should be seen in the compact components (Chiaberge et al. 2000). This would be alleviated if our model result is generally correct for BL Lacs, that the Lorentz factor for the beam is smaller than the Lorentz factor for the superluminal motion. On the other hand, such a general reduction in Lorentz factor for the beams will also reduce the Doppler factors, and that will exaggerate the difficulties that already exist in explaining very high brightness temperatures (Kovalev et al. 2005; Sokolovsky 2013).

6. CONCLUSIONS

The set of 110 images of BL Lac, observed with the VLBA at 15 GHz between 1999.2 and 2013.0, provides a remarkable view of the jet of this exceptional AGN. The jet has a strong quasi-stationary component (C7) at $r \approx 0.26$ mas from the core. Fast superluminal components appear to emanate from C7, in a manner strikingly similar to the ejection of fast shocks from the RCS that is seen in two-dimensional RMHD numerical simulations of jets that have a dominant, helical magnetic field. Furthermore, C7 is analogous to the component HST-1 in M87, which has been called an RCS. We therefore identify C7 as an RCS in the BL Lac jet.

A simple model is employed, one that uses the observed slowest and fastest moving components, with the assumption that they are manifestations of slow and fast magneto-acoustic waves propagating downstream on the relativistic beam. The model assumes that $\theta = 6^\circ$ and that the beam speed is constant. The result of fitting the model to the data is that the Lorentz factor for the beam is $\Gamma^{\rm gal}_{\rm beam} \approx 3.5$, and the fast magneto-acoustic wave has a speed relative to the beam of $\beta^{\rm beam}_{\rm Fwave} \approx 0.79$. This is mildly relativistic, with $\Gamma^{\rm beam}_{\rm Fwave} \approx 1.6$. These give the observed pattern speed $\beta_{\rm app} = 10$.

In the model, the Lorentz factor of the observed pattern is approximately three times larger than the Lorentz factor of the beam. This difference is in the correct sense to help alleviate difficulties in the BL Lac—FR I unification; but it is in the wrong sense to reduce the difficulties seen in explaining very high brightness temperatures.

We thank the anonymous referee whose comments substantially improved the paper. We are grateful to Ken Kellermann and the rest of the MOJAVE team for their comments and for their years of work in producing the data base that makes this work possible. T.H. was supported in part by a grant from the Jenny and Antti Wihuri foundation and by the Academy of Finland project number 267324. Y.Y.K. is partly supported by the Russian Foundation for Basic Research (project 13-02-12103), Research Program OFN-17 of the Division of Physics, Russian Academy of Sciences, and the Dynasty Foundation. A.B.P. was supported by the "Nonstationary processes in the Universe" Program of the Presidium of the Russian Academy of Sciences. T.G.A. acknowledges support by DFG project number Os 177/2-1. The VLBA is a facility of the National Radio Astronomy Observatory, a facility of the National Science Foundation that is operated under cooperative agreement with Associated Universities, Inc. The MOJAVE program is supported under NASA-Fermi grant 11-Fermi11-0019. Part of this research was carried out at the Jet Propulsion Laboratory, California Institute of Technology, under contract with the National Aeronautics and Space Administration. This research has made use of NASA's Astrophysics Data System.

APPENDIX

RELATIVISTIC ACOUSTIC MHD WAVES

Here we present the relativistic expressions for the slow and fast MHD wave counterparts to Equations (1) and (2). They are found in the same manner as the non-relativistic versions, but using the relativistic MHD equations instead (Meier 2012, Section 9.5.2.1): the equations are linearized about zero-velocity flow, with all quantities having small perturbations proportional

to $\exp[i(\boldsymbol{k}\cdot\boldsymbol{x}-\omega t)]$; keeping only acoustic perturbations ($\boldsymbol{k}\times\boldsymbol{\delta V}=0$) produces a quadratic equation in V^2 with two roots. Using the same form as the nonrelativistic versions in the text, the lower root gives the slow wave relativistic speed,

$$\beta_S=\pm\left\{\frac{1}{2}\left[\beta_{ms}^2\left\{1+\beta_c^2\cos^2\chi\right\}-\left(\beta_{ms}^4\left\{1+\beta_c^2\cos^2\chi\right\}^2-4\,\beta_s^2\beta_A^2\,\cos^2\chi\right)^{1/2}\right]\right\}^{1/2} \tag{A1}$$

and the upper root gives the fast wave relativistic speed,

$$\beta_F=\pm\left\{\frac{1}{2}\left[\beta_{ms}^2\left\{1+\beta_c^2\cos^2\chi\right\}+\left(\beta_{ms}^4\left\{1+\beta_c^2\cos^2\chi\right\}^2-4\,\beta_s^2\beta_A^2\,\cos^2\chi\right)^{1/2}\right]\right\}^{1/2} \tag{A2}$$

(Meier 2012, Equations (9.192)–(9.196)), where χ is the angle between the propagation direction $\boldsymbol{k}$ and the magnetic field direction. Note that β_S is the relativistic counterpart to the slow wave speed V_S in Section 4, while β_s is the counterpart to the plasma sound speed c_s. These expressions reduce to the nonrelativistic Equations (1) and (2) when terms of order higher than β^2 in the root (and higher than β^4 in the discriminant) are discarded. The relativistic cusp and magnetosound speeds in Equations A1 and A2 are

$$\beta_c=\beta_s\,\beta_A/\beta_{ms} \tag{A3}$$

$$\beta_{ms}=\left[\beta_A^2+\beta_s^2\left(1-\beta_A^2\right)\right]^{1/2} \tag{A4}$$

and the relativistic adiabatic sound and Alfvén speeds are

$$\beta_s=\left(\frac{\gamma p}{\rho c^2+\varepsilon+p}\right)^{1/2} \tag{A5}$$

$$\beta_A=\frac{B}{[4\pi(\rho c^2+\varepsilon+p+B^2/4\pi)]^{1/2}} \tag{A6}$$

where ε is the internal energy of the plasma; other quantities are defined in Section 4.

There are a few points of note. While the Alfvén speed $\beta_A\to 1$ as the magnetic pressure $B^2/8\pi\to\infty$, the same is not true for the adiabatic sound speed of a relativistic plasma ($\gamma=4/3$, $\varepsilon=3p$, $\rho c^2\ll p$): as $p\to\infty$, $\beta_s\to(1/3)^{1/2}\approx 0.577$ ($\Gamma_s\sim 1.22$). Sound waves in relativistic jets, therefore, may be limited to modest Lorentz factors. Note also the limitation in Equation (A4) on the sound speed contribution to the magnetosound speed when the magnetic field is strong and the Alfvén speed is relativistic. In that case, $\beta_{ms}\approx\beta_A$ and $\beta_c\approx\beta_s$ are good approximations. In the limit $\beta_A\to 1$, we always have $\beta_{ms}\to 1$, no matter what the value of β_s is.

Finally, while expressions (A1) and (A2) may look like they could exceed unity (and violate relativistic principles), they do not. The extrema of these quantities occur when $\beta_{ms}=\beta_A=1$, for any value of χ, and they are given by $\beta_S=\pm\beta_s\cos\chi$ and $\beta_F=\pm 1$.

REFERENCES

Agudo, I., Gómez, J.-L., Casadio, C., Cawthorne, T. V., & Roca-Sogorb, M. 2012, ApJ, 752, 92
Arshakian, T. G., León-Tavares, J., Lobanov, A. P., et al. 2010, MNRAS, 401, 1231
Asada, K., Inoue, M., Kameno, S., & Nagai, H. 2008, ApJ, 675, 79
Asada, K., Inoue, M., Uchida, Y., et al. 2002, PASJ, 54, L39
Bach, U., Villata, M., Raiteri, C. M., et al. 2006, A&A, 456, 105
Blandford, R. D. 1993, in Astrophysical Jets, Vol. 103, Astrophysics and Space Science Library ed. A. Ferrari & A. Pacholczyk (Cambridge: Cambridge Univ. Press), 15
Blandford, R. D., & Payne, D. G. 1982, MNRAS, 199, 883
Bromberg, O., & Levinson, A. 2009, ApJ, 699, 1274
Caproni, A., Abraham, Z., & Monteiro, H. 2013, MNRAS, 428, 280
Chang, C. S., Ros, E., Kovalev, Y. Y., & Lister, M. L. 2010, A&A, 515, A38
Cheung, C. C., Harris, D. E., & Stawarz, Ł. 2007, ApJL, 663, L65
Chiaberge, M., Celotti, A., Capetti, A., & Ghisellini, G. 2000, A&A, 358, 104
Clarke, D. A., Norman, M. L., & Burns, J. O. 1986, ApJL, 311, L63
Cohen, M. H., Lister, M. L., Homan, D. C., et al. 2007, ApJ, 658, 232
Falomo, R., Kotilainen, J. K., & Treves, A. 2002, ApJL, 569, L35
Gabuzda, D. C., Murray, E., & Cronin, P. 2004, MNRAS, 351, L89
Gabuzda, D. C., Pushkarev, A. B., & Cawthorne, T. V. 2000, MNRAS, 319, 1109
Gebhardt, K., Adams, J., Richstone, D., et al. 2011, ApJ, 729, 119
Gómez, J.-L., Marscher, A. P., Alberdi, A., Jorstad, S., & Agudo, I. 2001, ApJL, 561, L161
Gómez, J.-L., Marscher, A. P., Jorstad, S. G, Agudo, I., & Roca-Sogorb, M. 2008, ApJL, 681, L69
Grier, C. J., Peterson, B. M., Pogge, R. W., et al. 2012, ApJ, 755, 60
Homan, D. C., Kadler, M., Kellermann, K. I., et al. 2009, ApJ, 706, 1253
Hovatta, T., Aller, M. F., Aller, H. D., et al. 2014, AJ, in press (arXiv:1404.0014)
Hovatta, T., Lister, M. L., Aller, M. F., et al. 2012, AJ, 144, 105
Hovatta, T., Valtaoja, E., Tornikoski, M., & Lähteenmäki, A. 2009, A&A, 494, 527
Hughes, P. A., Aller, H. D., & Aller, M. F. 1989, ApJ, 341, 68
Jorstad, S. G., Marscher, A. P., Lister, M. L., et al. 2005, AJ, 130, 1418 (J05)
Komissarov, S. S. 1999, MNRAS, 308, 1069
Kovalev, Y. Y., Kellermann, K. I., Lister, M. L., et al. 2005, AJ, 130, 2473
Kovalev, Y. Y., Lobanov, A. P., Pushkarev, A. B., & Zensus, J. A. 2008, A&A, 483, 759
Krause, M., & Camenzind, M. 2001, A&A, 380, 789
León-Tavares, J., Lobanov, A. P., Chavushyan, V. H., et al. 2010, ApJ, 715, 355
Li, Z.-Y., Chiueh, T., & Begelman, M. C. 1992, ApJ, 394, 459
Lind, K. R., Payne, D. G., Meier, D. L., & Blandford, R. D. 1989, ApJ, 344, 89
Lister, M. L., Aller, M. F., Aller, H. D., et al. 2013, AJ, 146, 120 (L13)
Lister, M. L., Cohen, M. H., Homan, D. C., et al. 2009, AJ, 138, 1874
Lister, M. L., & Homan, D. C. 2005, AJ, 130, 1389
Lister, M. L., & Marscher, A. P. 1997, ApJ, 476, 572
Lyutikov, M., Pariev, V. I., & Gabuzda, D. C. 2005, MNRAS, 360, 869
Marscher, A. P., Jorstad, S. G., D'Arcangelo, F. D., et al. 2008, Natur, 452, 966
Meier, D. L. 2012, Black Hole Astrophysics: The Engine Paradigm (Berlin: Springer)
Meier, D. L. 2013, in EPJ Web of Conferences, Vol. 61, The Innermost Regions of Relativistic Jets and Their Magnetic Fields (Les Ulis, France: EDP Sciences), 01001
Moór, A., Frey, S., Lambert, S. B., Titov, O. A., & Bakos, J. 2011, AJ, 141, 178
Mutel, R. L., & Denn, G. R. 2005, ApJ, 623, 79 (MD05)
O'Sullivan, S. P., & Gabuzda, D. C. 2009a, MNRAS, 393, 429
O'Sullivan, S. P., & Gabuzda, D. C. 2009b, MNRAS, 400, 26
Paltani, S., & Türler, M. 2005, A&A, 435, 811
Polko, P., Meier, D. L., & Markoff, S. 2010, ApJ, 723, 1343
Polko, P., Meier, D. L., & Markoff, S. 2013, MNRAS, 428, 587
Polko, P., Meier, D. L., & Markoff, S. 2014, MNRAS, 438, 959
Pushkarev, A. B., Hovatta, T., Kovalev, Y. Y., et al. 2012, A&A, 545, A113
Pushkarev, A. B., Lister, M. L., Kovalev, Y. Y., & Savolainen, T. 2009, A&A, 507, L33
Savolainen, T., Wiik, K., Valtaoja, E., & Tornikoski, M. 2006, A&A, 446, 71
Sokolovsky, K. V. 2013, in Proc. 11th EVN Symp., 109
Sokolovsky, K. V., Kovalev, Y. Y., Pushkarev, A. B., & Lobanov, A. P. 2011, A&A, 532, A38
Stawarz, Ł., Aharonian, F., Kataoka, J., et al. 2006, MNRAS, 370, 981
Stirling, A. M., Cawthorne, T. V., Stevens, J. A., et al. 2003, MNRAS, 341, 405 (S03)
Tateyama, C. E. 2009, ApJ, 705, 877
Taylor, A. R., & Zavala, R. 2010, ApJL, 722, L183
Taylor, G. B., Hough, D. H., & Venturi, T. 2001, ApJ, 559, 703
Vlahakis, N., & Königl, A. 2003, ApJ, 596, 1080
Vlahakis, N., Tsinganos, K., Sauty, C., & Trussoni, E. 2000, MNRAS, 318, 417
Wandel, A., Peterson, B. M., & Malkan, M. A. 1999, ApJ, 526, 579
Woo, J.-H., & Urry, C. M. 2002, ApJ, 579, 530
Zamaninasab, M., Savolainen, T., Clausen-Brown, E., et al. 2013, MNRAS, 436, 3341
Zavala, R. T., & Taylor, G. B. 2002, ApJL, 566, L9
Zavala, R. T., & Taylor, G. B. 2005, ApJL, 626, L73